On the Importance of Noncrystalline Phases in Semicrystalline Electrospun Nanofibers

Foad Soleimani [a], Mozhdeh Mazaheri [a], Christian Pellerin [b,], and Reza Bagheri [a,*]*

[a] Polymeric Materials Research Group (PMRG), Department of Materials Science and Engineering, Sharif University of Technology, Azadi Ave., P.O. Box: 11365-9466, Tehran 14588, Iran

[b] Département de chimie, Université de Montréal, C.P. 6128, Succursale Centre-Ville, Montréal, Québec H3C 3J7, Canada

*Corresponding author. *E-mail*: c.pellerin@umontreal.ca (C. P.), rezabagh@sharif.edu (R. B.)

Table of Contents

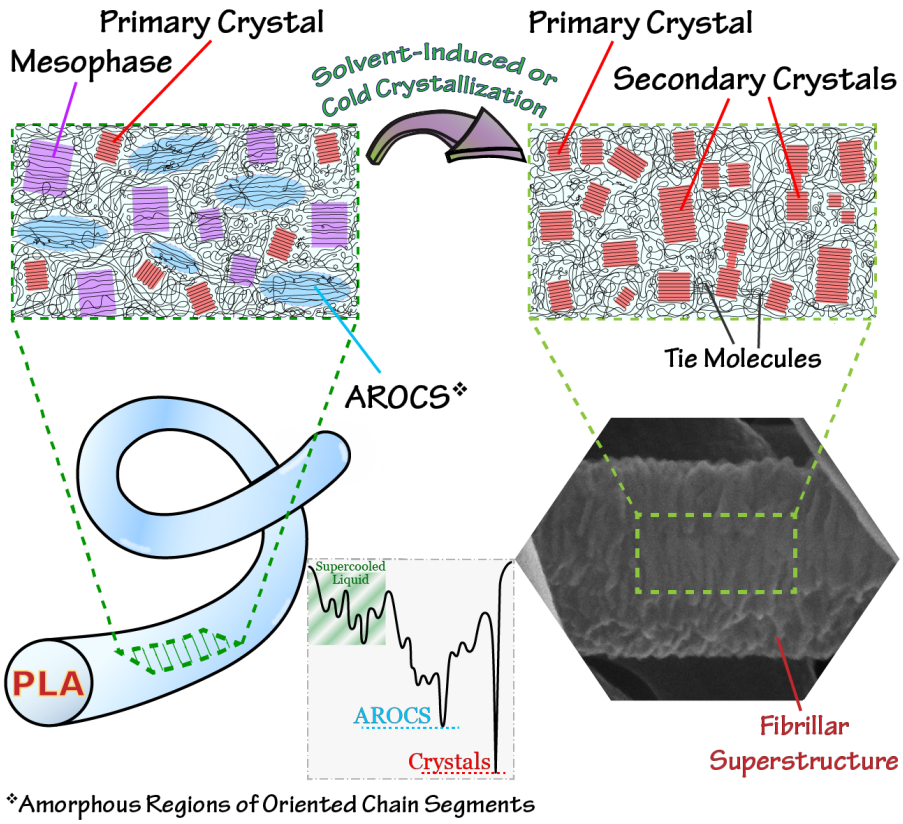

❖Amorphous Regions of Oriented Chain Segments

Abstract

Tailoring the properties of electrospun fibers requires a detailed understanding and control of their microstructure. We investigate the structure/property relationships in fabrics of randomly aligned fibers of polylactide, a prevalent biopolymer, either as-spun or after annealing and solvent-induced crystallization. In-depth characterization by field-emission scanning electron microscopy (FESEM), wide-angle X-ray diffraction (WAXD), attenuated total reflection Fourier transform infrared (ATR-FTIR), and modulated temperature differential scanning calorimetry (MT-DSC) reveals that the as-spun fibers comprise crystalline and mesomorphic phases, as well as oriented but mobile amorphous chain segments. These chains are mostly responsible for the low-temperature cold crystallization and for the recovery endotherm around the glass transition, while the mesophase transforms into crystals with nearly zero enthalpy. Such behaviors are attributed to high molecular orientation, which is further evidenced by unveiling a fibrillar superstructure in nanofibers. The thermodynamics and structural evolution under different conditions are described from an energy landscape perspective. Finally, we propose a micromechanism, based on a modified supramolecular model, which helps to elucidate the fibers' molecular dynamics.

Keywords: electrospinning; polylactide; molecular orientation; microstructure; mesophase.

1. Introduction

Over the past decades, a rising attention has focused on versatile and simple fabrication methods, like electrospinning, that allow designing materials with tailored properties for a wide range of applications.[1, 2] To make the most of electrospun (ES) fabrics, a thorough knowledge of their constituents' characteristics is essential.[3] An important, yet intricate characteristic of ES fibers is the nature and extent of their molecular orientation, which directly affects the microstructure and properties of individual fibers and their mats.[4] Many reports have outlined enhanced molecular orientation with a decrease in fiber diameter due to higher draw ratios, and to the lesser extent, confinement effects.[3-6] However, many details of the structure/property relationships remain unclear and are sometimes controversial for various systems.[3-5, 7, 8] Such discrepancies may arise from different intrinsic properties of polymers, fabrication parameters, or even from the characterization methods utilized at the fiber or at the mat scales.[4, 9]

Several attempts have been made to comprehend and conceptualize the underlying microstructure of ES fibers, most of which are extensively reviewed in the literature.[3, 4] This can be attained by means of various methods like infrared and Raman spectroscopies,[10-12] electron microscopy and diffraction,[13, 14] atomic force microscopy,[15, 16] X-ray scattering,[6] and mechanical[5] and thermal[17] analyses, to mention only a few. The formation of various oriented architectures has been suggested for different systems, such as fibrillar structures at the fiber surfaces[15, 18] or across the thinnest fibers,[14] nanofibrillar assemblies throughout the whole nanofibers,[11] a skin-core structure composed of a bulk-like isotropic core surrounded by highly-oriented chains in the skin,[16] a homogenous structure,[19] and supramolecular structures[20]

consisting of anisotropic “particles”, i.e. regions of densely-packed orientation-correlated amorphous chain segments which preferably orient along the fiber axis.[5] Among them, the skin-core structure is the most explored one for polymers with a glass transition temperature (T_g) higher than room temperature (RT). However, Xu et al.[21] recently reported the presence of cylinder-like substructures in ES polycarbonate fibers with characteristics analogous to the supramolecular structure originally proposed by Arinstein.[5] Yet, there are few reports about the formation of such oriented amorphous regions and their impact on the structure and properties of ES fibers.

Many of the above-mentioned studies have investigated individual fibers or bundles composed of aligned fibers to better understand their structural development in the course of spinning. While such preparation and investigation approaches are required to quantify molecular orientation, they also face drawbacks such as being complex, time-consuming and, in some cases, prone to characterization artifacts.[3] In the case of bundles, an excess molecular orientation could also be imposed by the collector due to fabrication parameters necessary to align the fibers macroscopically, e.g. a high take-up velocity on a rotating drum.[4] In this context, employing bulk characterization methods to study randomly-aligned fibers can complement studies on individual fibers by providing information on their structure and molecular dynamics in conditions akin to the spinning of the nonwoven mats that are used in the vast majority of applications.[7, 11, 22, 23]

A good model system to survey the structure/property relationships in ES fibers is polylactide (PLA), a widely used biosourced and biodegradable plastic,[24] because it manifests detectable

characteristics which are sensitive to the processing conditions.[13, 25, 26] Specifically, it was shown that molecular orientation within PLA fibers can lead to thermal and structural effects such as the appearance of an enthalpy recovery endotherm and the formation of a mesomorphic phase.[6, 17, 27] Very recently, Morel et al.[7] investigated the diffraction and thermal properties of PLA mats with different fiber diameters and deduced the formation of a skin-core structure. According to their later study on fibers subjected to solvent-induced crystallization (SIC), the skin would initially consist of a mesophase oriented along the fiber axis while the core would be amorphous.[13] Their investigations were conducted on single fibers, fabrics of aligned fibers, or fabrics of randomly-aligned fibers drawn to various strains prior to the analyses. Thus, it would be advantageous to systematically investigate PLA fabrics of randomly-aligned fibers which experienced no additional strains.

In the present work, we precisely investigate the structure/property relationship in PLA nonwoven fabrics by field-emission scanning electron microscopy (FESEM), wide-angle X-ray diffraction (WAXD), attenuated total reflection Fourier-transform infrared spectroscopy (ATR-FTIR), and modulated temperature differential scanning calorimetry (MT-DSC). Complementary post-treatments of the fabrics by thermal annealing and/or by submersion in a solvent which can swell PLA and induce crystallization without destroying the PLA structure[28] help revealing the microstructural evolution in the fibers. A model is proposed to describe the molecular dynamics of the as-spun and post-treated fibers and to rationalize the observed structure/property relationships.

2. Experimental Section

2.1. Materials, chemicals, and solution preparation

PLA granules (PLA 4032D, 1.2 – 1.6 mol.% D-isomer lactide, NatureWorks, USA) were used after annealing at 65 °C for 1 h. Dichloromethane (DCM, ≥ 99.0%, Merck), N,N-dimethylformamide (DMF, ≥ 99.0%, Merck), and formic acid (FA, 98 – 100%, Merck) were used as-received, as solvents or co-solvents. An appropriate amount of PLA granules were dissolved in DCM at RT using a magnetic stirrer. Then, DMF was added so that a solution of 7% w/v of PLA in the mixed solvent of DCM/DMF in 70:30 v/v ratio was obtained.

2.2. Electrospinning

Electrospinning was carried out on a Full Option Lab ES II (Nanoazma, Iran) apparatus. Details of fabrication variables are presented in **Table S1** of the Supporting Information. We tried to minimize any changes to the fabrics imposed by variation of processing conditions, e.g. humidity, temperature, needle inner diameter, and take-up velocity. The PLA solution was supplied through a blunt needle with large enough orifice (19-gauge) to prevent excess shear on the solution. The feeding rate was controlled such that a constant, uniform jet exited the spinneret with good quality of formation and flight towards the collector. The collector was a stainless steel drum (d = 80 mm) rotating at 50 rpm. Such a low rotation velocity ensures that mats of randomly-distributed fibers are collected and that the effects of high take-up speeds are minimized.[29] The prepared mat was immediately separated from the substrate and dried in a vacuum oven at 30 °C for 48 h. After drying, no significant amount of solvents was detected according to thermogravimetric analysis, TGA (**Figure S1**). For comparison, a thin film of a few micrometers thickness was prepared by casting the same solution on a glass petri-dish followed

by vacuum drying. The sample is named as L25SC. Also, an amorphous PLA film is prepared by quenching the molten polymer into ice-water.

2.3. Post-electrospinning treatments

Several samples were cut from the as-spun mat and subjected to annealing and/or solvent treatments described below. Thermal annealing was conducted in an air circulation oven (Heraeus UT 6 P) with a temperature control of ±1 °C. The samples were placed in the pre-heated oven and kept for 15 min, followed by air cooling to RT. Solvent treatment was conducted by dipping PLA fabrics in FA. Each sample was secured in a polypropylene frame and submerged in the solution under a fume hood. The solution was kept in a borosilicate glass tube capped with a silicone rubber tapered plug. After 90 min immersion, the samples were removed and dried in a vacuum oven as above. The samples were named as LT(FA), where T refers to the annealing temperature (25 for as-received samples, 65 for the samples annealed at 65 °C, and 90 for the samples annealed at 90 °C, respectively) and FA indicates a further solvent treatment in formic acid, if applicable. Detailed information on the samples is provided in **Table S2**.

2.4. Characterization techniques

TGA experiment was conducted on a METTLER TOLEDO TGA/DSC-1 thermogravimetric analyzer (Mettler-Toledo, Switzerland), at a heating rate of 10 °C min^{-1} using argon as the purge gas. FESEM was performed using a MIRA3 (TESCAN, Czech Republic) microscope operated at 20 kV. Mats were sputter-coated with platinum prior to analysis. Image analysis was done thanks to ImageJ software. WAXD patterns were collected on a Philips/PANalytical X'Pert PRO MPD

diffractometer (PANalytical BV, The Netherlands) using Cu-Kα radiation (λ = 1.542 Å) with an accelerating voltage of 35 kV. ATR-FTIR spectroscopy was conducted on an Equinox 55 FTIR spectrometer (Bruker Optics, Germany). MT-DSC thermograms were recorded on a DSC Q100 (TA Instruments, USA) under nitrogen atmosphere. Before tests, calibration of the heat flow and heat capacity values were performed using indium and sapphire as the references, respectively. The optimum analysis values for heating rate, modulation temperature, and modulation period in MT-DSC analyses were selected as 2 °C min^{-1}, 0.3 °C, and 60 s, respectively, in order to yield sufficient cycles of modulation during thermal events and eventually the most reliable results. Such values are under "heat-only" conditions.[30] The reliability of results was verified by repeating the experiments at least twice. The data were analyzed using TA Universal Analysis software.

3. Results and discussion

3.1. Characterization of ES PLA nanofibrous structure

A FESEM micrograph of a representative PLA fabric is shown in **Figure 1**. The fibers are randomly distributed at the very low drum rotation speed used, essentially flawless, and mostly uniform in their size along the fiber length. The fibers present a fairly narrow size distribution characterized by polydispersity indices of less than 0.12 for all samples prepared.

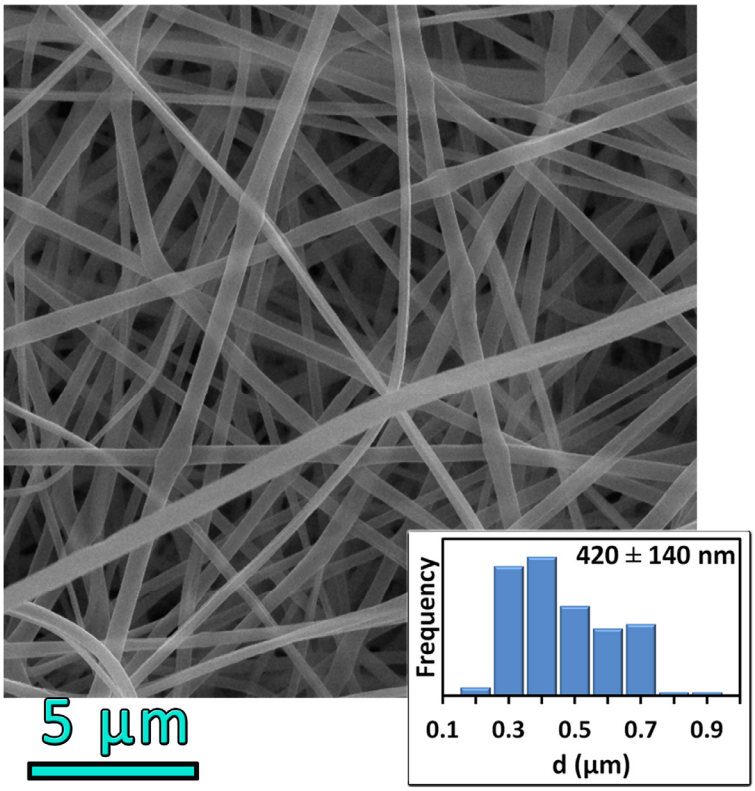

Figure 1. Characterization of L25 mat via FESEM imaging. The inset shows the histogram of the fibers diameter. Approximately 200 measurement were made and frequencies were calculated using Microsoft Excel's Analysis ToolPak.

The crystal structure, molecular conformation, and chain order of the as-spun mat is examined using WAXD and ATR-FTIR analyses. **Figure 2a** shows a WAXD pattern corrected for the instrumental background and fitted to Voigt profiles. The PLA mat demonstrates a semi-crystalline nature consisting of amorphous, mesomorphic, and crystalline phases. Three amorphous halos are discernible at 2θ of 15.0°, 21.2°, and 32.0° according to deconvolution of the signals. Two coincident peaks are centered at 2θ = 16.6° and correspond to the (1 1 0) or (2 0 0) reflections of the orthorhombic α or α' phases together, and to the mesomorphic phase,

respectively.[26, 31] The values of full width at half maximum (FWHM) of these peaks are 1.1° and 4.7°, respectively. As a measure of initial crystallinity and chain order in the as-spun fibers, the integrated intensities of the ordered phases' reflections are calculated in proportion to the area under the whole diffraction pattern. The contributions of crystalline and mesomorphic phases are ~ 2 % and 10 %, respectively. It is noteworthy that for such sample comprising a large amorphous content along with crystallites or lamellae of a few nanometers size, it is difficult to accurately separate the contributions of elastic and inelastic scattering and to eliminate the instrumental error in the recorded signal.[32]

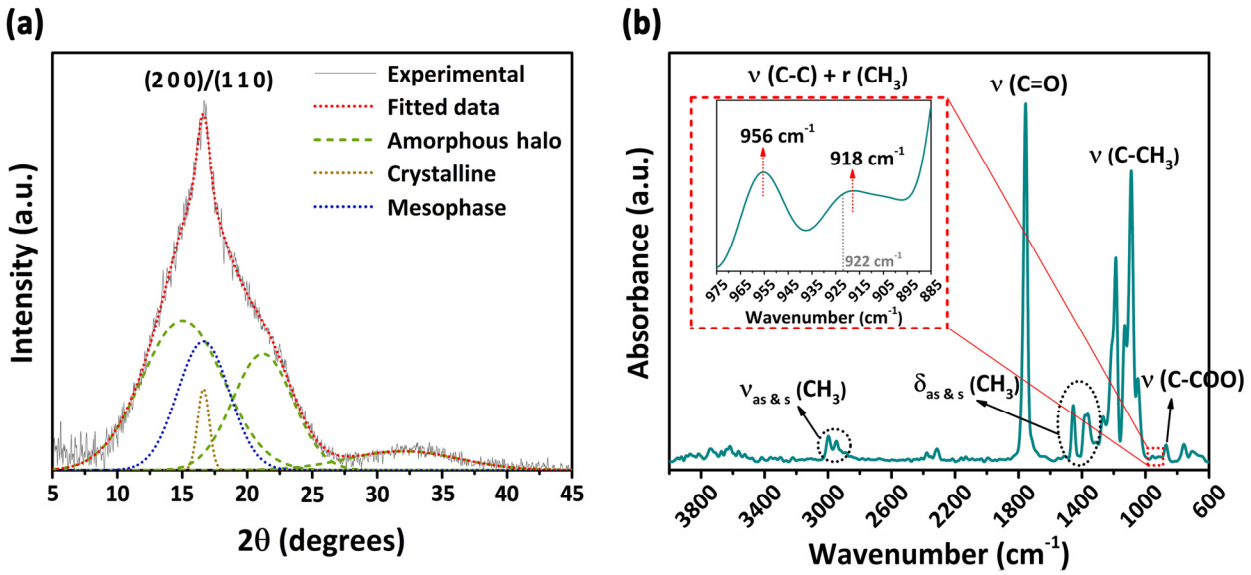

Figure 2. (a) WAXD pattern and (b) ATR-FTIR spectra of L25 mat.

An ATR-FTIR spectrum of the as-spun (L25) sample is shown in **Figure 2b**. The dominant phases can be discerned from the bands in C=O stretching region,[33] a close-up of which is reproduced in **Figure S2**. Previous reports suggested that a broad band centered at 1757 cm^{-1} would be

detected for amorphous PLA, while the crystalline phase of PLA shows a sharp band at 1759 cm^{-1} accompanied by several shoulders and band splitting.[34, 35] When the mesophase is formed, the band shifts to around 1753 cm^{-1}.[33, 35] Here, we observe a relatively sharp band centered at 1756 cm^{-1} with a negligible shoulder, consistent with the predominance of the amorphous phases noted in the WAXD pattern. While the band position is different from that of the mesophase, its relative sharpness suggests a higher chain order than that expected for a completely amorphous sample.

We also performed a close examination in the region of skeletal C−C stretching coupled with CH_3 rocking in the inset of **Figure 2b** where two bands are discernible at 956 and 918 cm^{-1}. In particular, the latter suggests chain order in the sample. Indeed, a band at 922 cm^{-1} is characteristic of the ordered 10_3 helical chain conformation and a shift in its position has been correlated to changes in conformational order and/or packing.[35] On this basis, several studies ascribed the band at 915 – 918 cm^{-1} to formation of the mesophase.[33, 35-38] In the present work, the band position at 918 cm^{-1} supports our WAXD and other FTIR indications for the presence of the mesophase along with the crystalline phase. The slight shift towards higher wavenumbers was previously attributed to better ordered chain conformation in the mesophase as a result of high molecular orientation in highly drawn PLA.[38] This could also be the case here, although the contribution of the crystalline phase to this band is also influential.

Zhang et al.[36] estimated the proportion of the ordered phases (crystal and mesophase) by dividing the integrated intensity of the ordered phase band (A_{918}) to the summation of peak areas of amorphous (A_{956}) and ordered phase bands. In our work, the relative content of

ordered phase is calculated as ~ 50 %, which is much higher than that obtained from WAXD results (12 %). A similar discrepancy was found in previous studies[7, 13] where the crystallinity of as-spun PLA fabrics was different when determined using different techniques. IR spectroscopy is sensitive to conformational order at the molecular scale while WAXD requires long-range order to produce diffraction peaks associated to ordered phases. The results thus suggest that the PLA fibers contain a large fraction of non-crystalline and non-mesomorphic but conformationally ordered chains as a result of high draw ratios during electrospinning. The peak at 918 cm^{-1} thus appears to represent not only the crystalline and mesomorphic phases, but also the contributions of locally-ordered amorphous chain segments. These chains, hereafter named as AROCS (amorphous regions of oriented chain segments), could be included in the above-mentioned supramolecular structures[5, 20] consisting of anisotropic "particles". In the next section, MT-DSC is used as a complementary and highly sensitive technique to investigate the details of the structure of ES fibers.[39]

3.2. Thermal behavior of ES fabric

Several features at the scale of molecules and molecular ensembles can be interpreted from DSC, such as chain confinement, crystallinity, and molecular orientation.[17, 26] A powerful counterpart to this analysis is MT-DSC, through which transitions otherwise hidden or overlapped by other processes can be perceived or distinguished.[40] **Figure 3a** shows the MT-DSC thermogram for the ES PLA mat heated from RT to above the melting region. For comparison, the thermogram of bulk PLA cast from the same solution is depicted in **Figure 3b**.

The thermal characteristics of all transitions observed are presented in **Table S3**, along with details on their determination.

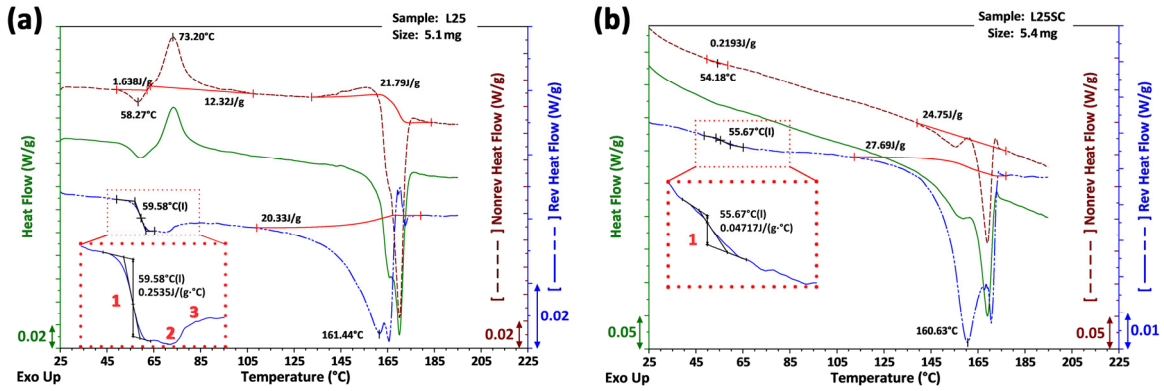

Figure 3. Investigation of thermal properties of PLA samples through MT-DSC: (a) as-spun mat (L25) and (b) solution-cast film (L25SC).

Upon heating the ES PLA, a glass transition (T_g, denoted by 1 in the insets) takes place at about 60 °C, accompanied by an endothermic event with a maximum at around 58 – 59 °C which is not detected for the PLA film. The presence of this endotherm normally reflects the enthalpy recovery of the amorphous chains due to thermal relaxation or physical aging below T_g.[26, 41] Some researchers rather claimed that molecular orientation in PLA fibers is responsible for the observation of such recovery peak.[17, 27] Besides, several reports attributed this endotherm to partial "melting" of the mesophase.[6, 26] One can see in the MT-DSC results that this peak is only present in the non-reversing signal, implying that it is a kinetic event and cannot be considered as "melting". This arises from the fact that in heat-only modulation, like the present analyses, any melting events necessarily show a sign in reversing signal.[30, 42, 43] Meanwhile, a second very

weak and shallow endotherm is observed in the reversing signal just above T_g (denoted by 2 in the inset of **Figure 3a**), which may represent the expected partial "melting" of the mesophase. We can envisage that the kinetic endotherm observed in our work is an enthalpy recovery peak that mostly arises out of the molecular orientation due to the shear exerted on the polymer jet below T_g during the spinning process. Such recovery occurs only in the mobile amorphous fraction (MAF) and could not be attributed to rigid amorphous fraction (RAF) or mesophase.[25, 44] We will bring further evidence on the origin of the recovery peak and its relation to the structural features of ES fibers in **Section 3.3.3**.

According to **Figure 3a**, the recovery event is followed by a significant cold crystallization (CC) exotherm at ~ 75 °C, well below the normal PLA CC peak above 100 °C. A low-temperature CC can result in the formation of the less-ordered α' phase rather than the ordered α crystals.[17, 34] Many studies attributed a decreased CC temperature to high molecular orientation within ES fibers leading to lower activation energy for crystallization.[13, 15, 17, 45] Concurrently, a decrease of C_p in the reversing signal is observed, denoted by 3 in the inset of **Figure 3a**, which can be linked to the transformation of less-constrained to more-constrained MAF and/or development of a RAF upon cold-crystallization.[46] Ma and coworkers[6] proposed that the whole process between ~ 45 and 85 °C in the reversing signal is an endothermic peak in the glass transition region. Notwithstanding, we believe that their observation should be revised as three consecutive events: a transition from glassy to supercooled liquid state which only occurs in the MAF, a weak melting of the mesophase, and a significant upward step due to cold-crystallization, during which the sample would shrink.

The final thermal event, observed for both the ES fibers and bulk PLA, is the melting of the crystalline phase at around 160 °C. As shown in **Table S3**, the melting enthalpy (ΔH_m) and total degree of crystallinity ($\chi_{c,tot}$) are lower for the ES sample than those for the solution-cast film. The high evaporation rate during spinning can kinetically freeze the chain conformation and reduce the crystallization capability of the ES sample. We note that $\chi_{c,tot}$ of ES PLA is comparable to the proportion of ordered phase obtained by ATR-FTIR, suggesting that most of the locally ordered chain segments would eventually crystallize during the DSC heating run.

The enthalpy of cold crystallization, ΔH_{cc}, shows the considerable contribution of cold-crystallized regions to the total crystallinity of the fibers. CC occurs most likely in the regions with highly-ordered chains that can easily reorganize. One can assume that such regions are uniformly distributed inside the fibers because their proportion is higher than that afforded by a thin skin at the surface of the fibers. It is also higher than the mesophase fraction calculated from the WAXD pattern, which implies that the chains that can undergo CC are not limited to the mesophase.

Also, the initial degree of crystallinity of the ES sample before the DSC ramp, χ_c, is much higher than that obtained by WAXD (26 % vs. 2 %). This value already excludes the contribution of chains that crystallized during CC so a possible crystallization prior to the CC event remains an open question. Indeed, it is still not clear which phases or regions contribute the most to the CC event, and how the mesophase can reorganize into the crystalline phase without the previously reported “melting” process.

3.3. Effect of post-treatment on structure/property relationships of ES mats

To further explore the microstructure of the fibers and survey their structure/property relationship, several samples were cut from the as-spun ES mats and were annealed to just above the recovery temperature (65 °C) or above CC (90 °C). These annealing temperatures were selected according to the MT-DSC thermograms for three different as-spun samples, magnified in the range of 40 - 100 °C in **Figure S3**. Other samples were treated in FA, either with or without previous annealing, to promote solvent-induced crystallization.

3.3.1. Microstructure of annealed and FA-treated fibers

FESEM micrographs of the post-treated samples illustrate how annealing and/or submerging in FA can affect the fibrous structure of the mat as well as the individual fibers (**Figures 4** and **5**). **Figure 4** shows that FA treatment results in a swelling of the fibers, compared to the as-spun mat, which is preserved after vacuum drying. The average fiber diameter increases from $\sim$ 420 ± 140 to $\sim$ 520 ± 150 nm after FA treatment (inset of **Figure 4a**). Although the fibers are fused in some spots and the network becomes tighter, the porous structure of the mat is generally preserved. An interesting morphology is revealed as a consequence of the interaction of PLA with FA (**Figure 4b**). In some fibers, the crystalline lamellae are distributed periodically along the fiber surface and connected by interfibrillar tie molecules, with their c-axis fairly parallel to the fiber axis. We will provide evidence below that this SIC is not restricted to the fibers' surfaces.

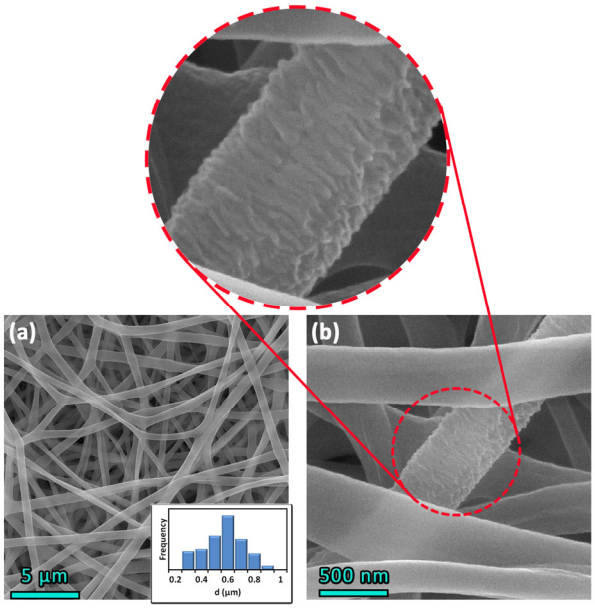

Figure 4. FESEM micrographs of FA-treated as-spun mat: (a) Low magnification image of L25FA with the inset showing the fibers size distribution; (b) Close investigation of the solvent-induced fibrillar superstructure.

Morel et al.[13] studied the SIC of PLA fibers in the presence of acetone, which is a PLA solvent. In such a case, it is not easy to differentiate the effect of a solvent on the bulk from that on the fibrous PLA. Here, we observed this phenomenon via a brief controlled exposure of PLA to FA. This polar protic organic acid (total Hansen solubility parameter, $\delta_t \approx 25$ $MPa^{1/2}$) has a lower capability of dissolving or swelling PLA ($\delta_t \approx 21.2$ $MPa^{1/2}$) compared to acetone ($\delta_t \approx 20.1$ $MPa^{1/2}$).[28] Consequently, it cannot easily penetrate and affect bulk PLA. In spite of this, our observations clearly show that FA can diffuse into PLA fibers. Thus, the structure of ES fibers should be less compact than that of bulk sample. Our findings also imply that there are regions of highly-oriented chain segments along the fiber's axis which can readily crystallize upon

exposure to FA. Morel et al.[13] reported that these regions are essentially the mesophase. Here, we suggest that ordered amorphous chains (AROCS) can also take part in SIC, in line with the proposed formation of ellipsoid-like anisotropic "particles"[5] as well as the formation of cylinder-like structures[21] parallel to the fibers axis.

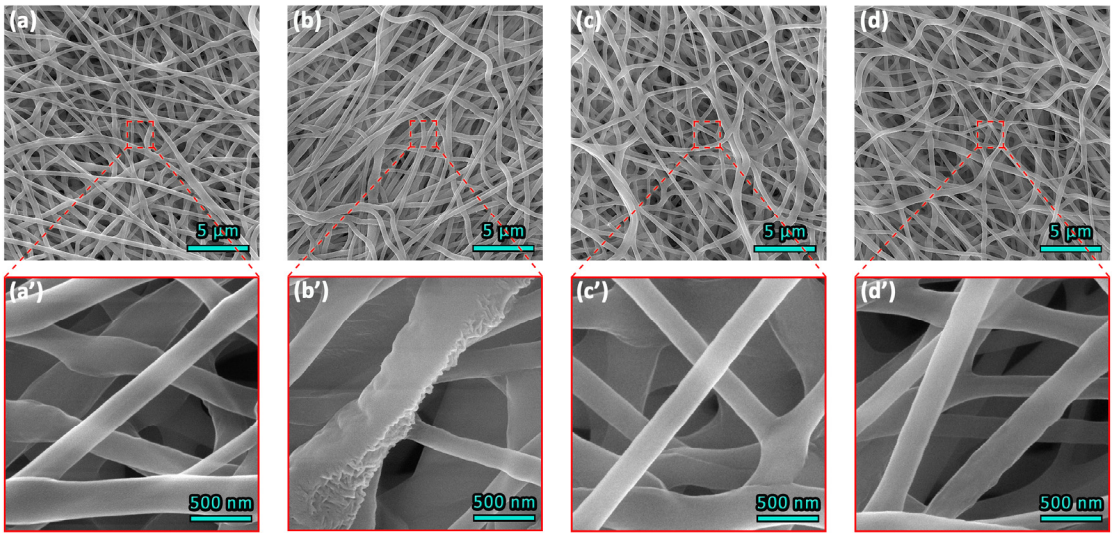

Figure 5. FESEM micrographs of annealed samples before and after FA treatment: (a, a') L65, (b, b') L65FA, (c, c') L90; (d, d') L90FA.

Annealing at 65 °C (L65), a temperature slightly above T_g but below T_{CC}, (**Figures 5a** and **a'**) brought about local distortion and protrusion of some fibers due to chain relaxation and surface tension. When additionally exposed to FA (L65FA), some annealed nanofibers become swollen and knitting of the fibers would occur (**Figure 5b**). A close investigation of the nanofibers in **Figure 5b'** reveals that FA can enter these fibers as for L25FA, although the fibrillar superstructure is less noticeable on the fiber surfaces. When the annealing temperature

exceeds the CC event (L90), the nanofibrous structure becomes more compact. As seen in **Figure 5c**, wavy nanofibers are evident in L90 and they are merged in some spots. However, in contrast to the other FA-treated samples, immersing L90 in FA has little to no effect on nanofibers' size and structure, except for their serration in some points (**Figures 5d** and **d'**). This implies that FA molecules could hardly penetrate the fibers.

3.3.2. Crystal structure of post-treated mats

WAXD patterns of annealed and FA-treated samples are presented in **Figure 6**. The appearance of a relatively sharp peak at $\sim$ 16.4° - 16.6° indicates that crystallization (α or α') occurs during either annealing or FA treatment. Except for L65, all treated samples show a high degree of crystallinity estimated as 47, 24, 46, 45, and 45 % for L25FA, L65, L65FA, L90, and L90FA, respectively, compared to only 2 % in the as-spun sample. These high values, close to the maximum degree of crystallinity in bulk PLA, indicate that CC and/or SIC can occur throughout the fibers and not only at their surface as observed by FESEM. Fitting the WAXD patterns reveals that thermal annealing leads to development of the less-ordered polymorph of α'-PLA, whose reflection is shifted to lower 2θ. In contrast, SIC in FA favors formation of more perfect and stable crystalline polymorph (α-PLA) in non-cold crystallized samples (L25FA and L65FA), analogous to the effect of acetone.[13] It is noteworthy that the peak deconvolution shows no indication of mesophase for any of the treated mats. One can therefore deduce that short-term annealing at just above T_g (L65), below the CC event, is sufficient to transform the mesophase into a crystalline structure.

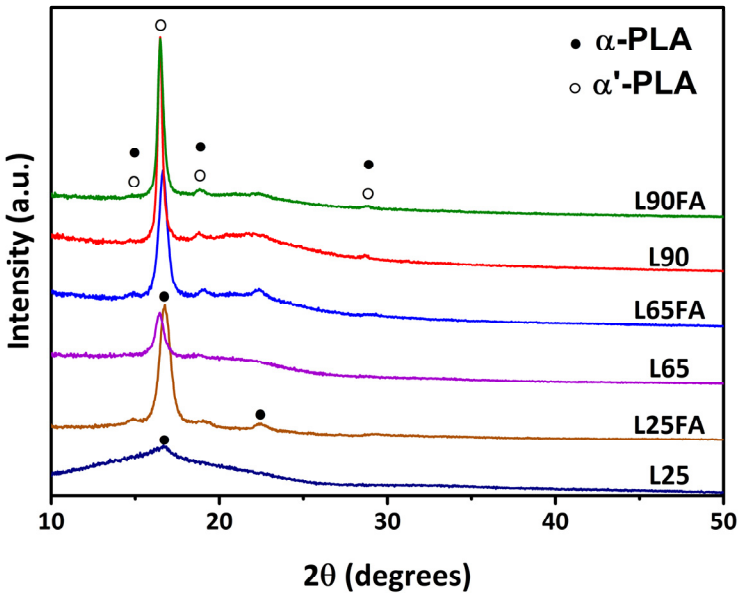

Figure 6. Diffraction patterns of samples processed by annealing and/or immersion in FA (L25FA, L65, L65FA, L90, and L90FA). The pattern of L25 sample is reproduced for comparison.

Values of FWHM of the most intense reflection are calculated as 0.8, 0.6, 0.6, 0.3, and 0.4° for L25FA, L65, L65FA, L90, and L90FA, respectively. In comparison, a broader peak (1.1°) was present for the as-spun L25 mat. This reduction in peak width can be ascribed to the formation of larger secondary crystallites and to the coalescence of existing lamellae during annealing or FA treatment.[13, 15] Similar to the FESEM observation, the WAXD results indicate that FA could negligibly affect the crystalline structure of L90. In particular, no shift is detected in the peaks position due to either crystal imperfection or α' → α transition, consistent with the absence of FA diffusion into the L90 structure. The case is rather different for the mat annealed at 65 °C. In contrast to L65, L65FA mostly consists of α-PLA, which shows that annealing at 65 °C results in a

fiber structure still loose enough to host FA molecules and allow at least a partial α' → α transition.

3.3.3. Thermal characteristics of post-treated ES mats

We also conducted MT-DSC analyses on the annealed and solvent-treated samples (**Figure 7**). FA-treated samples and samples annealed at above CC attained close to their maximum possible crystallinity. The calculated χ_C of post-treated samples, summarized in **Table 1**, are in good agreement with degrees of crystallinity obtained from WAXD results. It is seen that FA can induce slightly higher crystallinity than CC, perhaps because FA molecules facilitate the conformational changes of chain segments. The higher T_g of post-treated samples with higher crystalline fraction arises from the high level of ordering of their lamellae and the tie molecules connecting them, as evidenced by the discovery of a fibrillar superstructure.

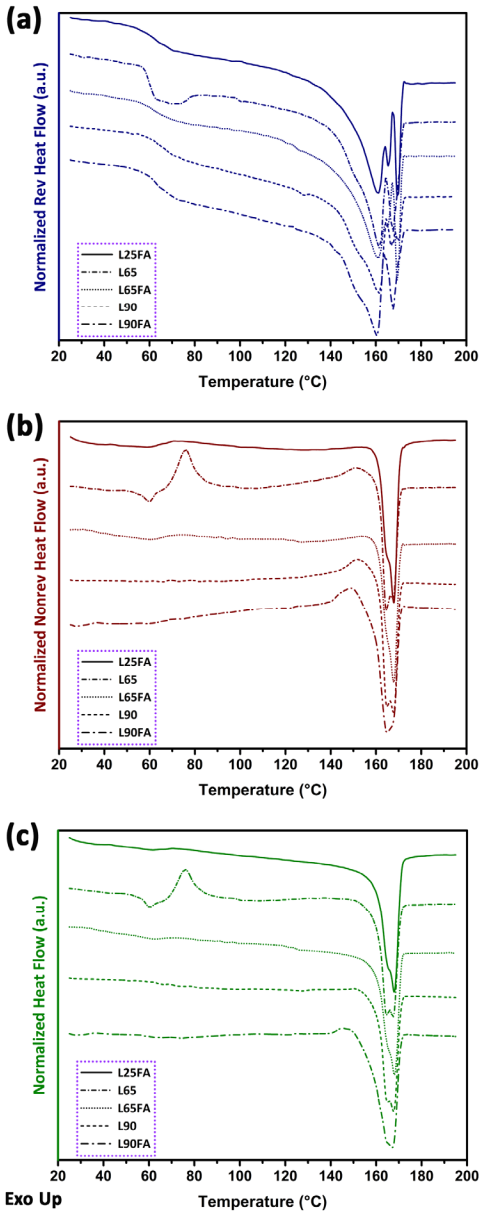

Figure 7. MT-DSC reversing (a), non-reversing (b), and total (c) signals of post-treated samples (L25FA, L65, L65FA, L90, and L90FA). Thermograms are vertically shifted and multiplied by a same factor for legibility.

Table 1. Summary of the thermal characteristics of post-treated samples comparing with as-spun mat

Sample	$T_{g,mid}$ (°C)	T_{rec} (°C)	T_{cc} (°C)	T_m (°C)	ΔH_{rec} ($J.g^{-1}$)	ΔH_{cc} ($J.g^{-1}$)	ΔH_m ($J.g^{-1}$)	χ_c (%)	$\chi_{c,tot}$ (%)
L25	59.5	58.6	75.1	161.0	1.8	12.3	40.4	26	44
L25FA	62.9	60.3	74.5	161.1	0.6	1.1	45.8	48	49
L65	59.6	59.9	75.9	161.4	1.6	12.0	42.1	28	45
L65FA	61.4	60.6	72.7	161.1	0.4	0.6	43.5	46	47
L90	63.1	-	-	161.4	-	-	41.9	45	45
L90FA	63.0	-	-	160.5	-	-	40.4	43	43

Figure 7b shows that a very weak recovery and CC can be discerned for L25FA and L65FA, while they are absent for L90 and L90FA. As expected, L65 experienced a considerable CC during the analysis. Furthermore, it shows a substantial enthalpy recovery endotherm, which was unexpected because the thermal history related to relaxation of chains should have been cleared through annealing at above the recovery temperature, i.e. 58.6 °C. In the WAXD pattern of L65 no reflection attributed to the mesophase was present. So, in contrast to some previous studies,[6, 7, 26, 37] both the enthalpy recovery and CC events should be ascribed to the presence of structural features other than the mesophase. Also, the contribution of analysis-related or

aging-related structural relaxation to the recovery peak at around 59 °C should be small. This can be inferred from the DSC thermogram of a quenched sample (**Figure S4**), where the enthalpy recovery is relatively small despite a higher MAF content. It is deduced that the recovery is most likely the consequence of conformational rearrangements due to high molecular orientation within the fibers.[47] At least parts of the amorphous chains in each fiber are rapidly solidified in a highly-oriented state, as proposed within the AROCS. Their solidification in such an ordered state makes them analogous to the chains structurally relaxed by aging below T_g in order to dissipate their frozen-in enthalpy toward the equilibrium glass.[17]

The hypothesis can be illustrated using the potential energy landscape (PEL) formalism (**Scheme 1**). Generally, structural relaxation during the aging process in the mobile amorphous portion of a polymer gives rise to the changes in the conformation of initially non-oriented chain segments towards attaining lower entropy and lower energy states.[41] When the polymer is heated to above T_g, the structural relaxation is readily recovered as the chains reach the supercooled liquid state. The observation of an endotherm concurrently with the glass transition is the most important sign of such process.[48] In the case of the AROCS, however, the chain segments are highly oriented upon their formation, so their conformation is originally in a lower energy state. As a consequence, they cannot easily explore the PEL and remain trapped in a deep local minimum. WAXD and MT-DSC results for L65 suggest that the AROCS are not destroyed when the sample is heated to just above T_g, so that these chain segments reach a higher local minimum energy and can return to their initial more stable energy state on cooling. The process is seemingly reversible, as illustrated in **Scheme 1**, unless the oriented chain segments attain high enough energies to overcome the barriers and explore the PEL for a deeper minimum, i.e.

formation of crystals with a defined enthalpy of cold crystallization. Any crystallization of the AROCS seems unlikely below T_g. This can rationalize the similarity of the ΔH_{CC}, ΔH_m, and χ_C values for L25 and L65 samples (**Table 1**). Further studies should be conducted on the aged ES mats as well as amorphous samples in order to compare ΔH_{rec} and also relaxation kinetics of the AROCS with those of the unconstrained amorphous chains through the relaxation process in the glassy state.

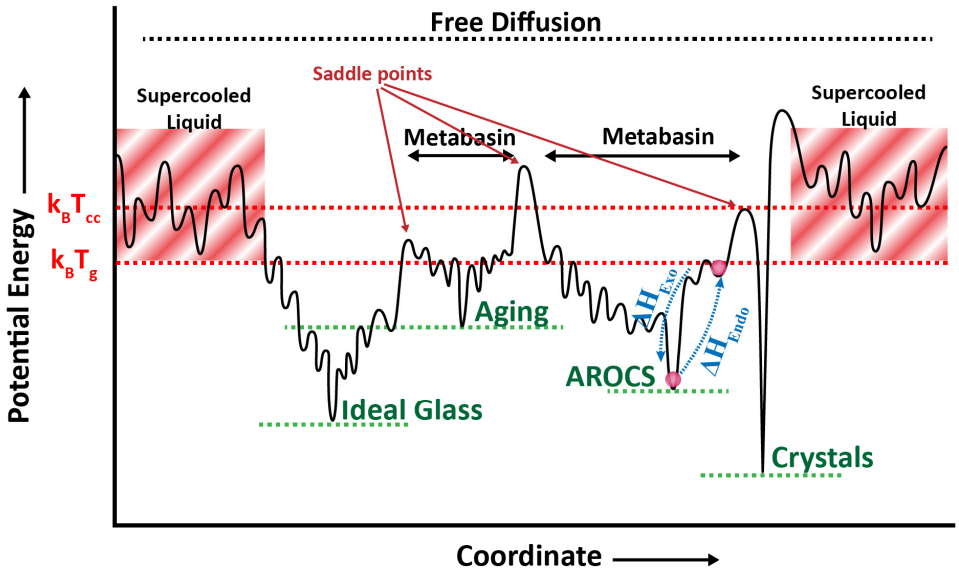

Scheme 1. Potential energy landscape for ES PLA fibers containing amorphous regions of oriented chain segments (AROCS). The energy landscape represents the possible energy states and structural transitions of the chains within the AROCS in comparison to those of the physically-aged chain segments.

The role of the AROCS on thermal characteristics is further surveyed by calculating the size of cooperative rearranging regions (CRRs) within ES fibers of L25 and L65 (**Figure 8**). CRRs' size is

calculated in the glass transition region and is ascribed merely to MAF or regions comprising MAF. The values of cooperativity length ($\xi_{T\alpha}$), represented in **Table S4**, show that CRRs' size of L25 (2.2 nm) and L65 (2.3 nm) is lower than that of the melt-quenched sample (2.8 nm) with almost completely amorphous structure (**Figure S5**). Monnier and coworkers[17] reported an increased CRR size in PLA fibers in comparison to quenched films, i.e. 3.6 against 2.8 nm. They attributed this observation to the cohesive role of the mesophase as anchoring points between macromolecules which increases intermolecular interactions. In contrast, Araujo et al.[22] reported a lower CRR size for polyacrylonitrile fibers, especially when higher molecular orientation was achieved in the fibers with smaller diameters. Our observations are in line with the latter and suggest that high molecular orientation is not eliminated after annealing at 65 °C.

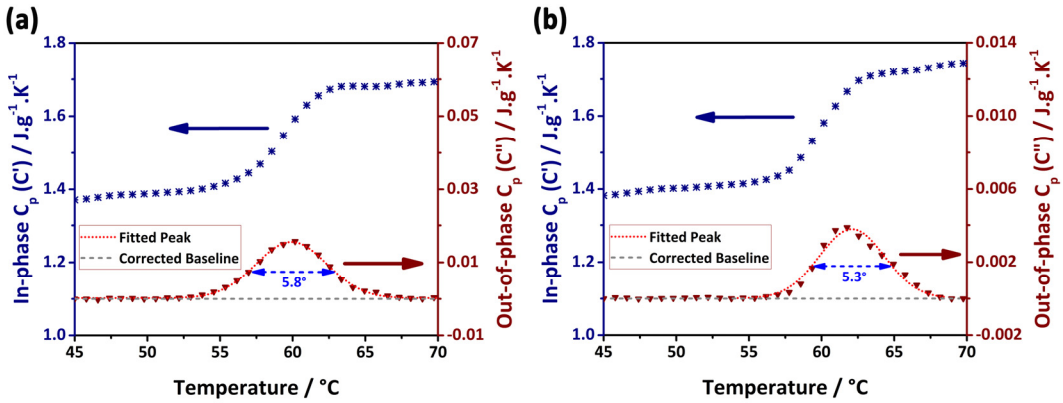

Figure 8. Variation of the in-phase and out-of-phase components of heat capacity at constant pressure in the range of dynamic glass transition temperature for (a) L25 and (b) L65 samples.

It is also seen in **Table S4** that the average temperature fluctuation of one CRR at T_g (δT) is almost equal for L25, L65, and the quenched sample. A higher δT is generally attributed to

hindered mobility of amorphous chains inside a CRR due to the geometrical confinement.[22] As the rearranging movements in a certain CRR are independent from those in other CRRs,[49] we can deduce that the presence of molecular orientation in ES fibers did not significantly alter the chain mobility within an individual CRR. This outcome can be interpreted by means of the supramolecular structure model.[5] The subchains in the AROCS, analogous to the directionally-correlated worm-like subchains in the "particles", are responsible for high molecular orientation, and their uniform distribution throughout the fibers decreases the cooperativity in comparison to a quenched sample. However, these AROCS would minimally confine the MAF or hinder the chains reorganization, because the AROCS are part of the MAF themselves.

3.4. Structural evolution during electrospinning and post-electrospinning treatments

By comparing χ_C of L25 with that of L65 in Table 1, one can suggest that the calculated value for L25 is indeed the summation of primary crystals initially present in the as-spun fibers and some secondary crystals formed upon heating to T_g. Indeed, mesophase reorganization into a crystalline phase apparently happens prior to or at the very early stage of CC. It was verified by WAXD that the mesophase crystallizes during a short annealing at 65 °C. So, we can consider the difference between χ_C and $\chi_{C,tot}$ as the portion of the AROCS which can crystallize during CC or SIC. This content is $\sim$ 18 %, verifying the significant contribution of the AROCS to the microstructure of the fibers.

Regarding the evolution of mesophase in the system, it seemingly crystallizes with almost no detectable thermal transition. We can propose two potential reasons: 1) the enthalpies of mesophase melting and its reorganization into crystals are both very low; 2) the mesophase

melting (in reversing signal) and reorganization (in non-reversing signal) events are overlapped by the glass transition and enthalpy recovery events, respectively. Due to the rather symmetric shape of these events in all recorded curves (**Figure S3**), the latter is unlikely. So, one may think of the transformation of mesophase to crystalline phase with nearly zero enthalpy. This is consistent with the observations of Stoclet and coworkers.[26] They showed that for PLA films drawn to high strains, mesophase melting would appear as a post-T_g endotherm around 70 - 75 °C with an enthalpy $\Delta H_m^{meso} \approx 70$ J g^{-1}. Afterwards, it can recrystallize into the stable α phase during a CC process. They observed that a higher applied strain, and thus a higher expected orientation, resulted in a smaller melting endotherm and in a narrower gap between the melting endotherm and CC exotherm. They also reported that the chain orientation remains even up to CC temperature in such a case and that the mesophase directly transforms to the crystalline phase without melting. To show the validity of our hypothesis, we depict a higher magnification of the reversing signal in the range of the glass transition and cold crystallization events in **Figure 9.** It clearly shows that no melting of mesophase is present in the glass transition region for neither L25 nor L65 samples. However, a very small post-T_g endotherm is observable beyond 65 °C, which can be attributed to the melting of a small portion of mesophase which is less cohesive.[26]

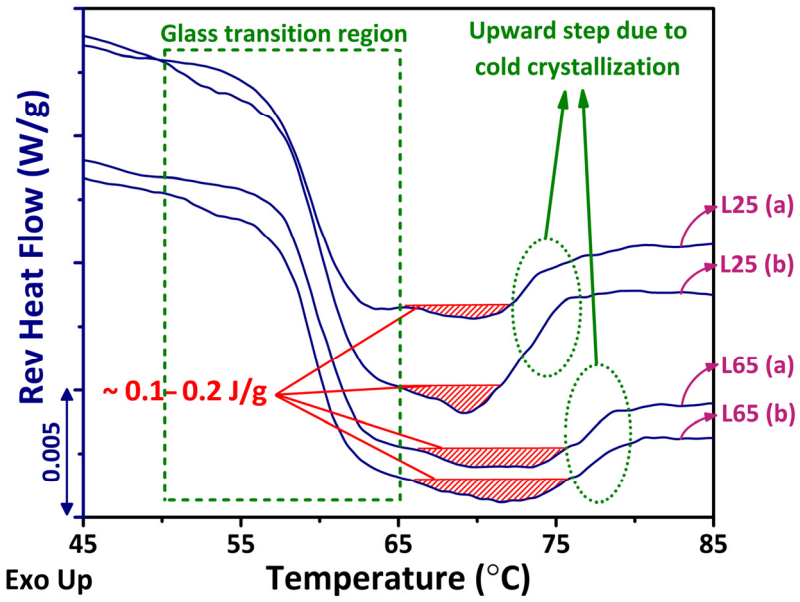

Figure 9. Magnification of MT-DSC reversing signal for two different as-spun (L25) and two different annealed (L65) samples. The hatched regions are seemingly attributed to the melting of some mesophase.

In our study, the mesophase content in the as-spun samples is estimated by WAXD to be around 10 %. This content should have led to a much larger endotherm around T_g, considering the proposed ΔH_m^{meso}, if this peak was indeed due to mesophase melting. Moreover, the endotherm maximum is located slightly below T_g, in contrast to the study of Stoclet and coworkers.[26] Last but not least, the endotherm is only detected in the non-reversing signal, which implies that the connected thermal event is not a heat capacity-related one, like "melting". We can deduce that the mesophase reorganizes into the crystalline state directly without a sequence of melting and subsequent crystallization. Similar to the suggestion of Stoclet et al.[26] for the samples prepared via high draw ratios, heating the as-spun mats first

leads to the reorganization of the mesophase into the less-ordered α' phase (**Figure 6**) with almost zero enthalpy of crystallization (**Figures 7 and S3**). The higher ordering of the mesophase in fibers, compared to drawn films, can be inferred from its WAXD peak at a larger angle than that observed by Stoclet et al.,[31] i.e. 16.6° compared to 16.2°. So, the molecular dynamics just above the glass transition favor the transition of the mesophase to α' both thermodynamically and kinetically.

Based on our observations, a schematic representation of ES fibers' plausible inner architecture is depicted in **Scheme 2** for as-spun and annealed/FA-treated samples. The inner part of the as-spun fibers contains a substantial fraction of anisotropic AROCS and mesophase, in addition to the crystals and unoriented amorphous chains. The formation of a skin-core structure[9, 13] is rejected because the contribution of the AROCS and mesophase is higher than plausible if they were restricted to a thin skin. In the meantime, the model shows the heterogeneity of the structure throughout the fibers, in compliance with previous studies.[5, 16] When an ES PLA mat is annealed at just above T_g, the mesophase would reorganize into less-perfect α' crystals while the anisotropic AROCS would remain almost unchanged. Annealing at above CC or submersion in a suitable solvent stimulates crystallization in nearly all ordered regions, so that crystallinity reaches close to the maximum possible value.

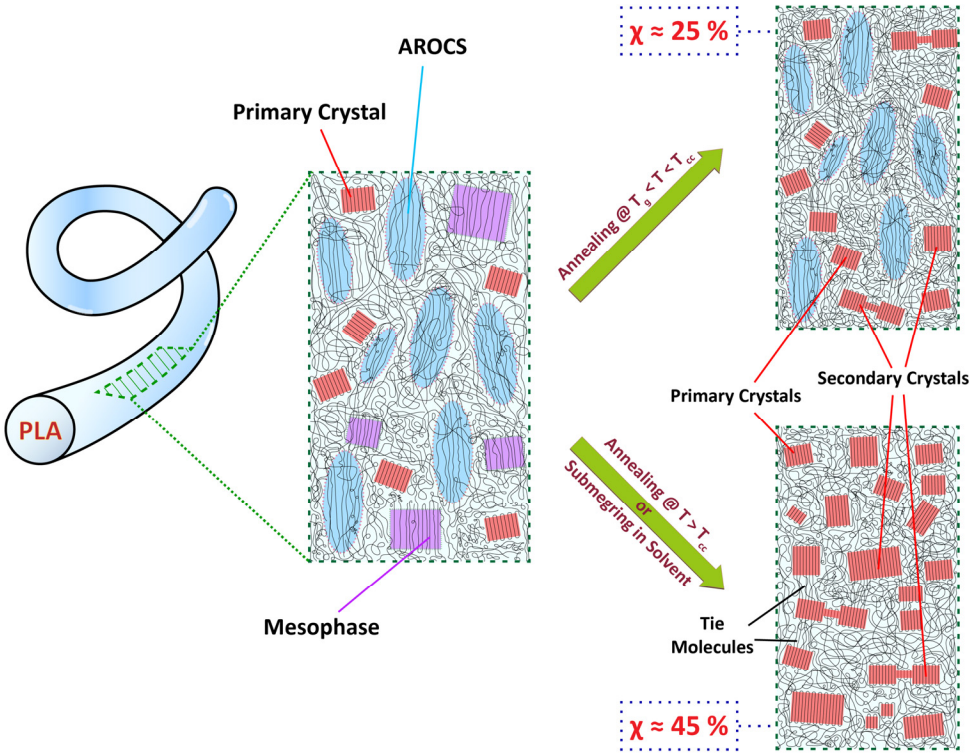

Scheme 2. Proposed model for the inner architecture of ES semi-crystalline PLA fibers, upon formation and after post-treatment.

4. Conclusions

PLA nanofiber mats were fabricated under controlled electrospinning conditions. Through the in-depth investigations by WAXD, ATR-FTIR, and MT-DSC, the formation of the regions of highly-oriented amorphous chain segments (AROCS) was revealed along with a mesomorphic phase. To validate this conjecture, ES PLA mats were subjected to post-treatments by annealing and/or submersion in FA. It was found that upon annealing the mats to just above T_g, the mesophase reorganizes into less-perfect crystalline α' phase. The anisotropic AROCS appear responsible for

the enthalpy recovery peak near T_g and were inclined to crystallize by cold-crystallization upon annealing at higher temperature and by SIC in the presence of FA. In both cases, the ES fabrics nearly reached their maximum possible crystallinity. A fibrillar superstructure is observed in the FA-treated mats, which helps elucidating the molecular dynamics within the fibers and investigating their likely chain orientation. We finally proposed a model of the inner microstructure of the as-spun, solvent-crystallized, and cold-crystallized PLA fibers.

ASSOCIATED CONTENT

Supporting Information. Experimental details including electrospinning variables, preparation procedure, and selection of proper annealing temperature; TGA curve for as-spun mat; details of calculation of thermal characteristics and cooperativity length; summary of some samples thermal properties; and thermal properties of a quenched PLA sample.

AUTHOR INFORMATION

Corresponding Authors

Christian Pellerin - Département de chimie, Université de Montréal, C.P. 6128, Succursale Centre-Ville, Montréal, QC H3C 3J7, Canada; orcid.org/0000-0001-6144-1318; E-mail address: c.pellerin@umontreal.ca.

Reza Bagheri - Polymeric Materials Research Group (PMRG), Department of Materials Science and Engineering, Sharif University of Technology, Azadi Ave., Tehran, P.O. Box: 11365-9466, Iran; orcid.org/0000-0003-1868-401X; E-mail address: rezabagh@sharif.edu.

Authors

Foad Soleimani - Polymeric Materials Research Group (PMRG), Department of Materials Science and Engineering, Sharif University of Technology, Azadi Ave., Tehran, P.O. Box: 11365-9466, Iran; orcid.org/0000-0001-7752-9795.

Mozhdeh Mazaheri - Polymeric Materials Research Group (PMRG), Department of Materials Science and Engineering, Sharif University of Technology, Azadi Ave., Tehran, P.O. Box: 11365-9466, Iran; orcid.org/0000-0001-9585-783X.

Notes

The authors declare no competing financial interest.

ACKNOWLEDGMENTS

R.B. received funding from the Research and Technology Office of Sharif University of Technology (Grant No. G940301). C.P. acknowledges the financial support of the Natural Sciences and Engineering Research Council of Canada (RGPIN-2020-05098). The authors express their gratitude to Dr. Rasool Lesan-Khosh, Arnaud Laramée, and Parviz Nasoodi for their scientific and technical assistance.

References

(1) Lim, S. H.; Mao, H.-Q. Electrospun scaffolds for stem cell engineering. *Advanced drug delivery reviews* **2009,** 61 (12), 1084-1096.

(2) Fakirov, S. Nano-size polymers. *Cham: Springer International Publishing* **2016**, DOI: 10.1007/978-3-319-39715-3.

(3) Papkov, D.; Delpouve, N.; Delbreilh, L.; Araujo, S.; Stockdale, T.; Mamedov, S.; Maleckis, K.; Zou, Y.; Andalib, M. N.; Dargent, E. Quantifying polymer chain orientation in strong and tough nanofibers with low crystallinity: toward next generation nanostructured superfibers. *ACS nano* **2019,** 13 (5), 4893-4927.

(4) Richard-Lacroix, M.; Pellerin, C. Molecular orientation in electrospun fibers: from mats to single fibers. *Macromolecules* **2013,** 46 (24), 9473-9493.

(5) Arinstein, A. Confinement mechanism of electrospun polymer nanofiber reinforcement. *Journal of Polymer Science Part B: Polymer Physics* **2013,** 51 (9), 756-763.

(6) Ma, Q.; Pyda, M.; Mao, B.; Cebe, P. Relationship between the rigid amorphous phase and mesophase in electrospun fibers. *Polymer* **2013,** 54 (10), 2544-2554.

(7) Morel, A.; Domaschke, S.; Kumaran, V. U.; Alexeev, D.; Sadeghpour, A.; Ramakrishna, S. N.; Ferguson, S. J.; Rossi, R. M.; Mazza, E.; Ehret, A. E. Correlating diameter, mechanical and structural properties of poly (L-lactide) fibres from needleless electrospinning. *Acta Biomaterialia* **2018,** 81, 169-183.

(8) Ji, Y.; Li, C.; Wang, G.; Koo, J.; Ge, S.; Li, B.; Jiang, J.; Herzberg, B.; Klein, T.; Chen, S. Confinement-induced super strong PS/MWNT composite nanofibers. *EPL (Europhysics Letters)* **2008,** 84 (5), 56002.

(9) Baji, A.; Mai, Y.-W.; Wong, S.-C.; Abtahi, M.; Chen, P. Electrospinning of polymer nanofibers: effects on oriented morphology, structures and tensile properties. *Composites science and technology* **2010,** 70 (5), 703-718.

(10) Richard-Lacroix, M.; Pellerin, C. Orientation and partial disentanglement in individual electrospun fibers: diameter dependence and correlation with mechanical properties. *Macromolecules* **2015,** 48 (13), 4511-4519.

(11) Kongkhlang, T.; Tashiro, K.; Kotaki, M.; Chirachanchai, S. Electrospinning as a new technique to control the crystal morphology and molecular orientation of polyoxymethylene nanofibers. *Journal of the American Chemical Society* **2008,** 130 (46), 15460-15466.

(12) Papkov, D.; Pellerin, C.; Dzenis, Y. A. Polarized Raman analysis of polymer chain orientation in ultrafine individual nanofibers with variable low crystallinity. *Macromolecules* **2018,** 51 (21), 8746-8751.

(13) Morel, A.; Oberle, S. C.; Ulrich, S.; Yazgan, G.; Spano, F.; Ferguson, S. J.; Fortunato, G.; Rossi, R. M. Revealing non-crystalline polymer superstructures within electrospun fibers through solvent-induced phase rearrangements. *Nanoscale* **2019,** 11 (36), 16788-16800.

(14) Yoshioka, T.; Dersch, R.; Tsuji, M.; Schaper, A. K. Orientation analysis of individual electrospun PE nanofibers by transmission electron microscopy. *Polymer* **2010,** 51 (11), 2383-2389.

(15) Tan, E. P.; Lim, C. Effects of annealing on the structural and mechanical properties of electrospun polymeric nanofibres. *Nanotechnology* **2006,** 17 (10), 2649.

(16) Stachewicz, U.; Bailey, R. J.; Wang, W.; Barber, A. H. Size dependent mechanical properties of electrospun polymer fibers from a composite structure. *Polymer* **2012,** 53 (22), 5132-5137.

(17) Monnier, X.; Delpouve, N.; Basson, N.; Guinault, A.; Domenek, S.; Saiter, A.; Mallon, P.; Dargent, E. Molecular dynamics in electrospun amorphous plasticized polylactide fibers. *Polymer* **2015,** 73, 68-78.

(18) Lim, C.; Tan, E.; Ng, S. Effects of crystalline morphology on the tensile properties of electrospun polymer nanofibers. *Applied Physics Letters* **2008,** 92 (14), 141908.

(19) Arshad, S. N.; Naraghi, M.; Chasiotis, I. Strong carbon nanofibers from electrospun polyacrylonitrile. *Carbon* **2011,** 49 (5), 1710-1719.

(20) Arinstein, A.; Burman, M.; Gendelman, O.; Zussman, E. Effect of supramolecular structure on polymer nanofibre elasticity. *Nature nanotechnology* **2007,** 2 (1), 59.

(21) Xu, Y.; Gao, Y.; Wang, X.; Jiang, J.; Hou, J.; Li, Q. Internal structure of amorphous electrospun nanofiber: Oriented molecular chains. *Macromolecular Materials and Engineering* **2017,** 302 (7), 1700054.

(22) Araujo, S.; Delpouve, N.; Delbreilh, L.; Papkov, D.; Dzenis, Y.; Dargent, E. Dielectric and calorimetric signatures of chain orientation in strong and tough ultrafine electrospun polyacrylonitrile. *Polymer* **2019,** 178, 121638.

(23) Wong, D.; Andriyana, A.; Ang, B. C.; Verron, E. Surface morphology and mechanical response of randomly oriented electrospun nanofibrous membrane. *Polymer Testing* **2016,** 53, 108-115.

(24) Fakirov, S., *Biodegradable polyesters*. John Wiley & Sons: 2015.

(25) Delpouve, N.; Saiter, A.; Dargent, E. Cooperativity length evolution during crystallization of poly (lactic acid). *European polymer journal* **2011,** 47 (12), 2414-2423.

(26) Stoclet, G.; Seguela, R.; Lefebvre, J.-M.; Rochas, C. New insights on the strain-induced mesophase of poly (d, l-lactide): in situ WAXS and DSC study of the thermo-mechanical stability. *Macromolecules* **2010,** 43 (17), 7228-7237.

(27) Puchalski, M.; Kwolek, S.; Szparaga, G.; Chrzanowski, M.; Krucińska, I. Investigation of the influence of PLA molecular structure on the crystalline forms (α'and α) and mechanical properties of wet spinning fibres. *Polymers* **2017,** 9 (1), 18.

(28) Sato, S.; Gondo, D.; Wada, T.; Kanehashi, S.; Nagai, K. Effects of various liquid organic solvents on solvent-induced crystallization of amorphous poly (lactic acid) film. *Journal of applied polymer science* **2013,** 129 (3), 1607-1617.

(29) Zhang, X.; Nakagawa, R.; Chan, K. H. K.; Kotaki, M. Mechanical property enhancement of polylactide nanofibers through optimization of molecular weight, electrospinning conditions, and stereocomplexation. *Macromolecules* **2012,** 45 (13), 5494-5500.

(30) Thomas, L. C. Modulated DSC® Paper# 6 Measurement of Initial Crystallinity in Semi-crystalline Polymers. *TA Instruments* **2005**, 1-9.

(31) Stoclet, G.; Seguela, R.; Vanmansart, C.; Rochas, C.; Lefebvre, J.-M. WAXS study of the structural reorganization of semi-crystalline polylactide under tensile drawing. *Polymer* **2012,** 53 (2), 519-528.

(32) Londoño-Restrepo, S. M.; Jeronimo-Cruz, R.; Millán-Malo, B. M.; Rivera-Muñoz, E. M.; Rodriguez-García, M. E. Effect of the nano crystal size on the X-ray diffraction patterns of biogenic hydroxyapatite from human, bovine, and porcine bones. *Scientific reports* **2019,** 9 (1), 1-12.

(33) Zhang, J.; Duan, Y.; Domb, A. J.; Ozaki, Y. PLLA mesophase and its phase transition behavior in the PLLA− PEG− PLLA copolymer as revealed by infrared spectroscopy. *Macromolecules* **2010,** 43 (9), 4240-4246.

(34) Pan, P.; Inoue, Y. Polymorphism and isomorphism in biodegradable polyesters. *Progress in Polymer Science* **2009,** 34 (7), 605-640.

(35) Koido, S.; Kawai, T.; Kuroda, S.; Nishida, K.; Kanaya, T.; Kato, M.; Kurose, T.; Nakajima, K. Mesomorphic phase formation of plasticized poly (l-lactic acid). *Journal of Applied Polymer Science* **2014,** 131 (2), 39762.

(36) Zhang, T.; Hu, J.; Duan, Y.; Pi, F.; Zhang, J. Physical aging enhanced mesomorphic structure in melt-quenched poly (L-lactic acid). *The Journal of Physical Chemistry B* **2011,** 115 (47), 13835-13841.

(37) Lv, R.; Na, B.; Tian, N.; Zou, S.; Li, Z.; Jiang, S. Mesophase formation and its thermal transition in the stretched glassy polylactide revealed by infrared spectroscopy. *Polymer* **2011,** 52 (21), 4979-4984.

(38) Wang, Y.; Li, M.; Wang, K.; Shao, C.; Li, Q.; Shen, C. Unusual structural evolution of poly (lactic acid) upon annealing in the presence of an initially oriented mesophase. *Soft Matter* **2014,** 10 (10), 1512-1518.

(39) Gómez-Pachón, E. Y.; Sánchez-Arévalo, F. M.; Sabina, F. J.; Maciel-Cerda, A.; Campos, R. M.; Batina, N.; Morales-Reyes, I.; Vera-Graziano, R. Characterisation and modelling of the elastic properties of poly (lactic acid) nanofibre scaffolds. *Journal of Materials Science* **2013,** 48 (23), 8308-8319.

(40) Reading, M.; Luget, A.; Wilson, R. Modulated differential scanning calorimetry. *Thermochimica acta* **1994,** 238, 295-307.

(41) Surana, R.; Pyne, A.; Rani, M.; Suryanarayanan, R. Measurement of enthalpic relaxation by differential scanning calorimetry—effect of experimental conditions. *Thermochimica acta* **2005,** 433 (1-2), 173-182.

(42) Lacey, A. A.; Price, D. M.; Reading, M., Theory and practice of modulated temperature differential scanning calorimetry. In *Modulated Temperature Differential Scanning Calorimetry*, Springer: Dordrecht, The Netherlands 2006; pp 1-81.

(43) Wunderlich, B. Reversible crystallization and the rigid–amorphous phase in semicrystalline macromolecules. *Progress in polymer science* **2003,** 28 (3), 383-450.

(44) Monnier, X.; Chevalier, L.; Esposito, A.; Fernandez-Ballester, L.; Saiter, A.; Dargent, E. Local and segmental motions of the mobile amorphous fraction in semi-crystalline polylactide crystallized under quiescent and flow-induced conditions. *Polymer* **2017,** 126, 141-151.

(45) Zong, X.; Kim, K.; Fang, D.; Ran, S.; Hsiao, B. S.; Chu, B. Structure and process relationship of electrospun bioabsorbable nanofiber membranes. *Polymer* **2002,** 43 (16), 4403-4412.

(46) Righetti, M. C. Crystallization of polymers investigated by temperature-modulated DSC. *Materials* **2017,** 10 (4), 442.

(47) Aou, K.; Kang, S.; Hsu, S. L. Morphological study on thermal shrinkage and dimensional stability associated with oriented poly (lactic acid). *Macromolecules* **2005,** 38 (18), 7730-7735.

(48) Cangialosi, D. Dynamics and thermodynamics of polymer glasses. *Journal of Physics: Condensed Matter* **2014,** 26 (15), 153101.

(49) Donth, E. Characteristic length of the glass transition. *Journal of Polymer Science Part B: Polymer Physics* **1996,** 34 (17), 2881-2892.